A)	HH18-1		HH18-2		HH18-3		HH18-4		HH18-5		HH18 Average	
	Right	Left	Right	Left	Right	Left	Right	Left	Right	Left	**Right**	**Left**
II	0.6±0.07%	1.5±0.37%	3.2±1.32%	3.7±1.98%	3.5±0.18%	4.1±0.43%	0.9±0.03%	0.2±0.05%	3.4±0.66%	4.3±0.17%	**2.3±0.45%**	**2.8±0.60%**
III	**47.0±1.44%**	36.0±1.08%	**47.1±1.26%**	38.7±1.61%	35.5±0.28%	**46.5±0.20%**	33.3±0.18%	**59.2±0.23%**	35.1±0.24%	**43.3±0.33%**	**39.6±0.68%**	**44.7±0.16%**
IV	6.8±0.04%	8.1±0.09%	3.0±0.15%	4.3±0.28%	5.7±0.10%	4.7±0.11%	2.1±0.04%	4.3±0.14%	5.0±0.13%	8.7±0.18%	**4.5±0.09%**	**6.0±0.16%**
B)	HH24-1		HH24-2		HH24-3		HH24-4		HH24-5		HH24 Average	
	Right	Left	Right	Left	Right	Left	Right	Left	Right	Left	**Right**	**Left**
III	12.7±3.51%	9.4±2.28%	18.0±3.74%	18.4±2.62%	**33.7±0.66%**	17.3±0.21%	13.0±6.01%	**38.8±6.37%**	**32.3±1.83%**	17.2±1.99%	**21.9±3.15%**	**20.2±2.69%**
IV	**32.4±5.80%**	10.7±1.93%	7.5±8.57%	**25.4±4.14%**	28.4±0.31%	13.8±0.42%	8.8±5.66%	29.3±4.50%	30.8±2.29%	9.6±2.44%	**21.6±4.53%**	**17.8±2.69%**
VI	25.4±2.12%	9.5±2.86%	19.6±2.42%	11.1±0.52%	5.2±0.30%	1.6±0.11%	3.6±0.55%	6.5±1.49%	5.9±0.81%	4.2±0.42%	**11.9±1.24%**	**6.6±1.08%**
C)	HH26-1 (fast)		HH26-2		HH26-3		HH26-4		HH26-5 (slow)		HH26 Average	
	Right	Left	Right	Left	Right	Left	Right	Left	Right	Left	**Right**	**Left**
III	6.9±0.40%	8.5±0.06%	6.8±1.16%	13.7±0.90%	7.5±1.20%	7.3±1.31%	9.6±0.96%	19.5±1.14%	**26.8±2.53%**	16.8±0.12%	**11.5±1.25%**	**13.2±0.71%**
IV	5.3±0.14%	19.2±0.16%	5.5±1.04%	10.9±1.20%	5.1±0.96%	8.5±1.58%	7.3±0.84%	9.5±0.85%	21.4±0.81%	10.4±1.14%	**8.9±0.76%**	**11.7±0.99%**
VI	**46.7±0.39**	12.6±0.07%	**32.1±2.48%**	30.9±1.79%	**53.4±6.52%**	18.8±1.44%	**35.6±2.67%**	19.0±0.41%	14.9±0.81%	9.8±9.79%	**36.5±2.57%**	**18.2±2.70%**

Table S1. Subject-specific percent flow values per arch of HH18, HH24, HH26 embryos

Mean flow distribution (over the length of a cardiac cycle) values for HH18 (A) HH24 (B) and HH26 (C) embryos. The arch that takes up the largest percentage of flow (bolded) varies substantially between embryos and across stages. Distributions averaged across the population are shown on the right.

Significant WSS Morphology Trends

Area				Dmax				Dmin			
PAA	equation	R^2 value	P-Value	PAA	equation	R^2 value	P-Value	PAA	equation	R^2 value	P-Value
IIIR	Y = -287083*X - 20.80	0.639	0.006	IIIL	Y = -10727*X - 48.77	0.858	0.0001	IIIL	Y = 28096*X - 4.253	0.7591	0.001
IVR	Y = 257104*X - 105.2	0.5712	0.012	IIIR	Y = -2685*X - 19.52	0.427	0.0406	IIIR	Y = 12444*X - 19.81	0.5028	0.0217
IVL	Y = 380920*X - 102.3	0.8647	< 0.0001	IVL	Y = 7482*X - 82.03	0.666	0.004	IVR	Y = 14150*X - 96.28	0.7867	0.0006
								IVL	Y = 15348*X - 85.25	0.417	0.0437
IIIR	Y = -202013*X - 32.20	0.4558	0.032	IIIR	Y = -6948*X - 48.81	0.505	0.0213				
IVL	Y = -254604*X + 4.286	0.6689	0.004	IVL	Y = -8118*X - 3.918	0.479	0.0266	IIIR	Y = -14145*X - 17.68	0.4596	0.0312
VIR	Y = -675337*X + 19.24	0.4206	0.043	VIR	Y = -29229*X + 154.1	0.859	0.0001	IVR	Y = -22393*X - 28.65	0.7259	0.0017
VIL	Y = -424674*X + 79.47	0.774	8E-04	VIL	Y = -22981*X + 87.50	0.64	0.0054	IVL	Y = -23960*X + 9.923	0.6636	0.0041
								VIR	Y = -27998*X + 130.1	0.9141	< 0.0001
								VIL	Y = -26444*X + 83.04	0.8472	0.0002

Significant Pulsatility Morphology Trends

Area				Dmax				Dmin			
PAA	equation	R^2 value	P-Value	PAA	equation	R^2 value	P-Value	PAA	equation	R^2 value	P-Value
				IIIL	Y = 25803*X + 88.23	0.769	0.0009	IIIL	Y = -61081*X - 14.78	0.555	0.0134
IVL	Y = -450602*X - 12.78	0.4766	0.027	VIL	Y = -26601*X + 89.90	0.711	0.0022	IVL	Y = -47296*X - 0.1343	0.5881	0.0096
VIL	Y = -431664*X + 70.87	0.6628	0.004					VIL	Y = -26655*X + 73.89	0.7135	0.0021

Table S2: Equations and values for statistically significant linear regression of Figures 5 and 7. HH18-HH24 trends (black), HH24-HH26 trends (blue).

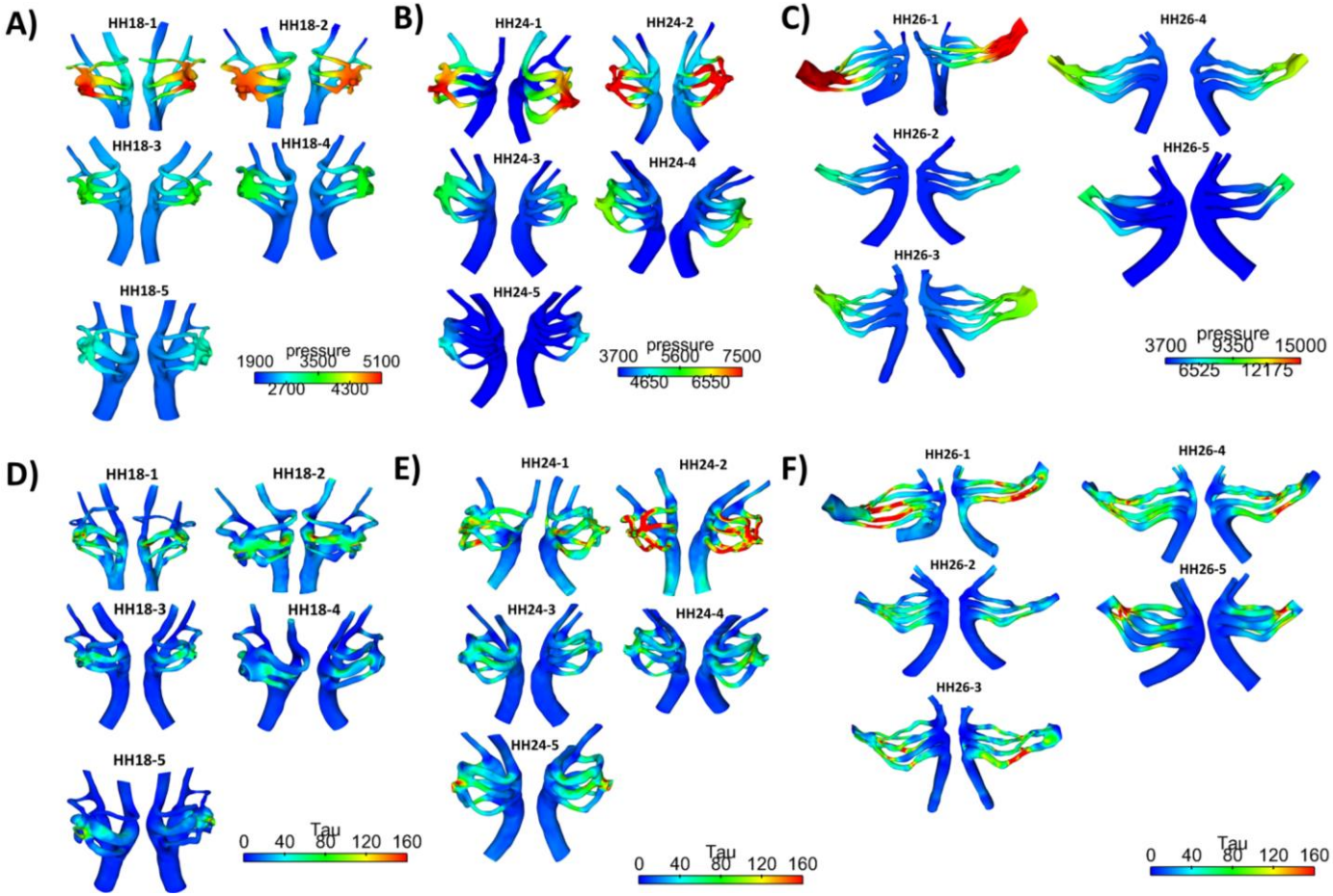

Figure S1: HH18 HH24 and HH26 Pressure and WSS maps

Pressure distributions (dyne·cm^{-2}) across HH18 embryos at peak flow (A), HH24 embryos (B) HH26 embryos (C) and the corresponding WSS maps (dyne·cm^{-2}) HH18 (D), HH24(E), HH26 (F). Though the magnitude of the pressure changes from stage to stages, it is greatest at the inlet and through the aortic sac, before being dissipated through the arches. Peaks in WSS can be found at the inlet junction and large PAAIII for HH18 embryos, at the inlet junction and several arches for HH24 embryos. Three distinct WSS patterns can be seen within the HH26 cohort.

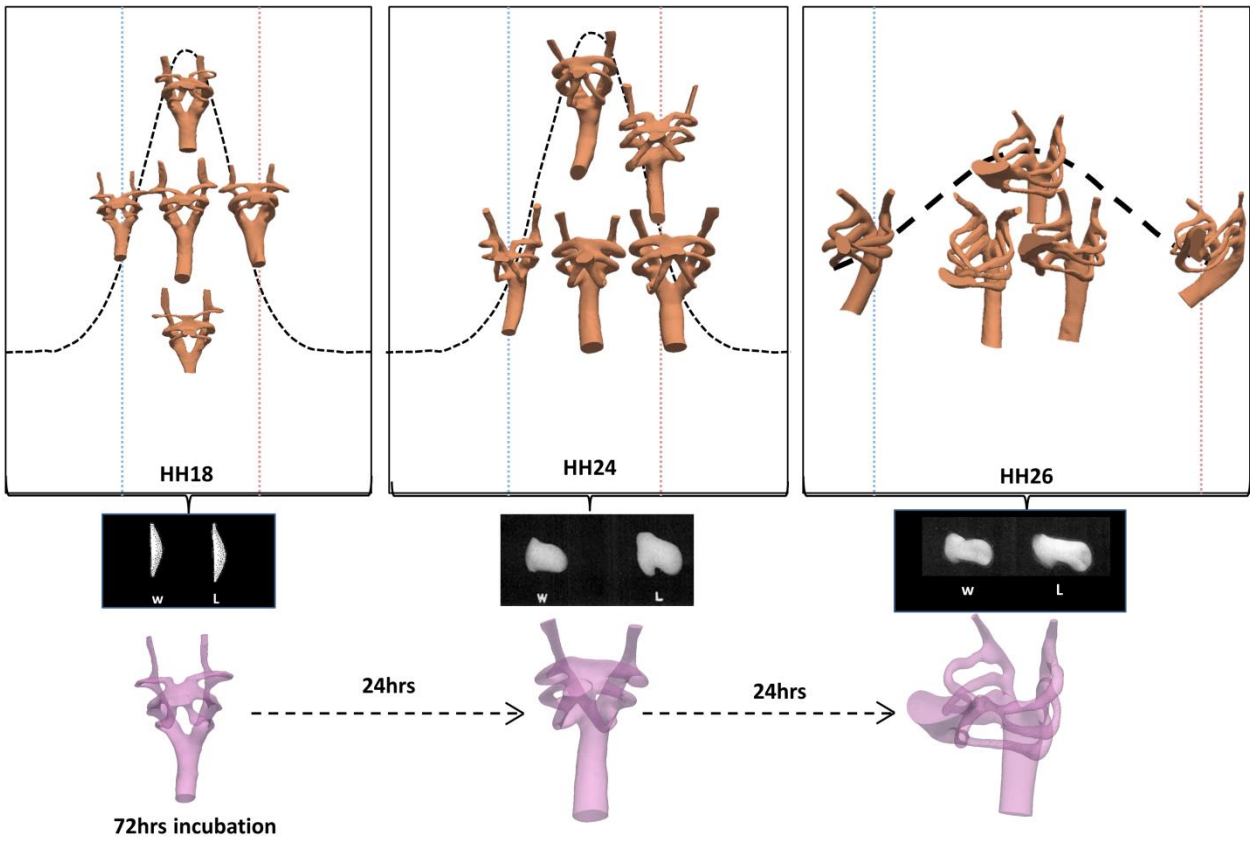

Figure S2: Morphological Embryo Variability

Embryos were staged based on the classic Hamburger Hamilton stages of development (Hamburger & Hamilton, 1951). While much attention was given to the "fast" and "slow" HH26 configurations, each of the three stages can be divided into arch morphology subgroups that represent a different level of maturation at the level of the PAAs. Vertical lines mark what can be considered the upper (red) and lower (blue) specification limit for each stage. For HH18 embryos, subgroups were determined based on arch IV diameter and overall IV arch volume. Similarly, HH24 embryo subgroups were determined based on curved arch length, and overall distance from the DOA bifurcation to the OFT inlet. HH26 subgroups are much more pronounced due to the substantial morphological changes taking place with OFT septation, rotation and elongation. A clear bell curve exists at each of the HH stages, with the most noticeable and informative differences occurring during the HH26 stage. Wing (w) and limb (l) are the two parameters used for staging (adapted from Hamburger and Hamilton 1951).

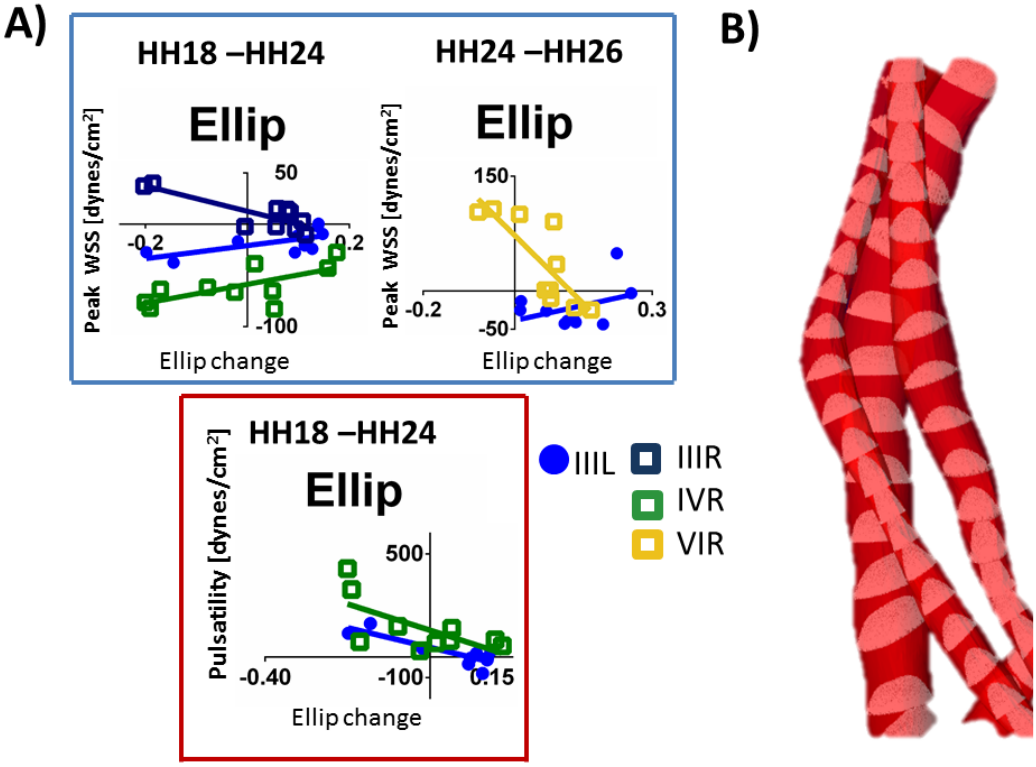

C)

WSS Ellipticity Trends			
PAA	equation	R^2 value	P-Value
IIIL	Y = -170.7*X + 19.27	0.8607	0.0001
IIIR	Y = -123.8*X + 12.74	0.7144	0.0021
IVR	Y = -79.24*X + 31.45	0.6158	0.0072
IIIL	Y = -217.5*X + 6.917	0.8786	< 0.0001
VIR	Y = -249.7*X + 14.06	0.7251	0.0018

WSS Pulsatility Trends			
PAA	equation	R^2 value	P-Value
IVR	Y = -636.4*X + 130.3	0.4448	0.0352
IIIL	Y = -478.1*X + 47.06	0.725	0.0018

Figure S3: Ellipticity Morphological Change Summary

A) Linear regressions were performed to highlight hemodynamic-ellipicity correlations for WSS at peak flow and Ellipticity. Both graphs show change in X and Y values. B) Flow profile along the arch arteries subject-specific non-idealized geometries. Note how vessels have a parabolic-like profile in two of the arches (Poiseuille flow) though the profile becomes slightly skewed depending on its position along the arch. C) P-values and equations for trends of (A).

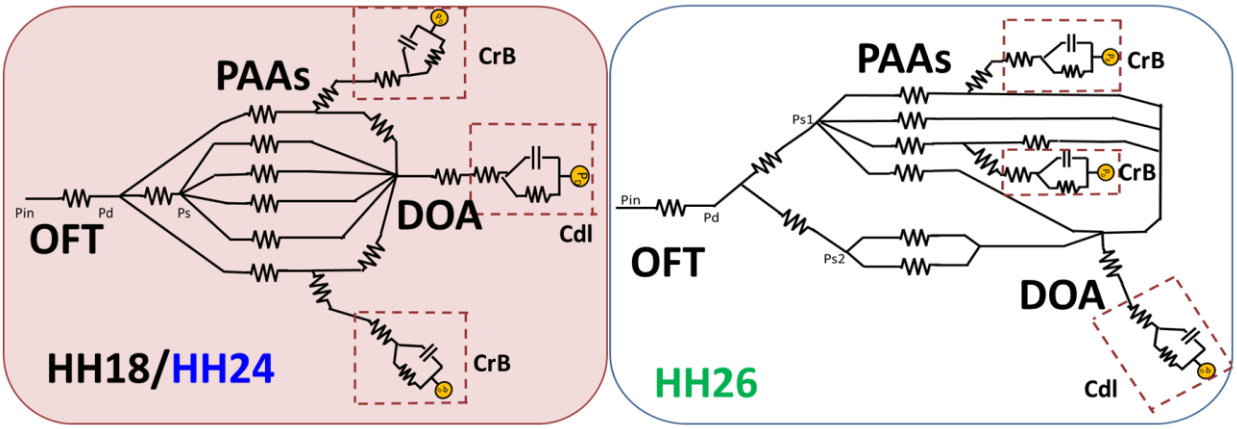

Figure S4: PAA Lumped parameter models.

Lumped parameter representation of HH18 and HH24 embryos (left). Only the numbering of the arch arteries themselves will change between stages. HH26 lumped parameter network (right) must take into account OFT septation which placed the caudal arches on a different branch than the cranial arches. Dashes lines (red) outline 0D bounds of the multiscale 3D-0D model. Ps (HH18/HH24) refers to pressure from aortic sac, Ps1 and Ps2 (HH26) represent pressure at the end of the septated OFT junctions. Pd is the pressure associated with the distal most part of the small OFT entrance. Pin, inlet pressure. CrB-cranial branch, Cdl, caudal branch.

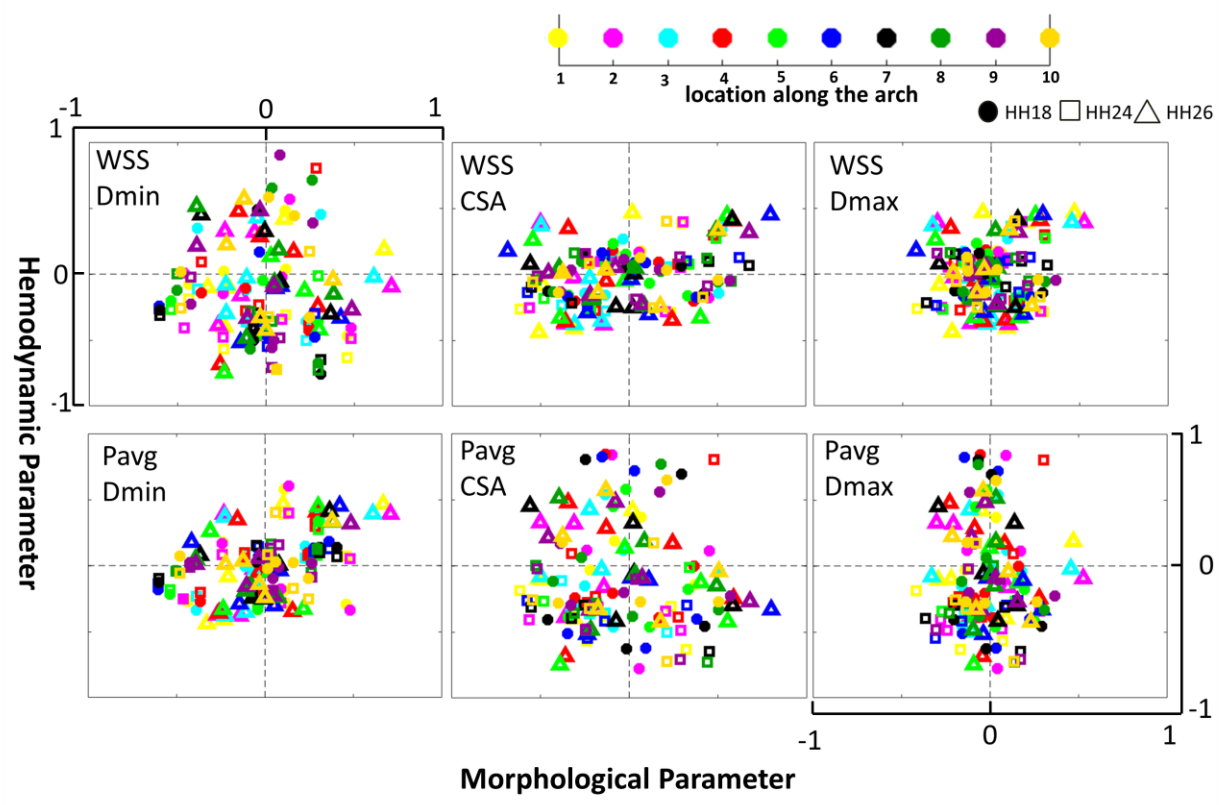

Figure S5: PAA IIIR Variation versus Variation Dynamics

Representative deviation from mean graphs for PAA IIIR indicate the number of sections evaluated per hemodynamic-morphology category and how some factors varied more than others. Peak WSS and Pavg deviation from mean (Y-axis) versus the deviation from D_{min}, Area, and D_{max} (X-axis) are shown for each of the ten sections along the embryo and each of the five embryos per stage. A selected range of -1 to 1 is shown to facilitate marker and trend identification. Least variability per region is broken down in Table1.

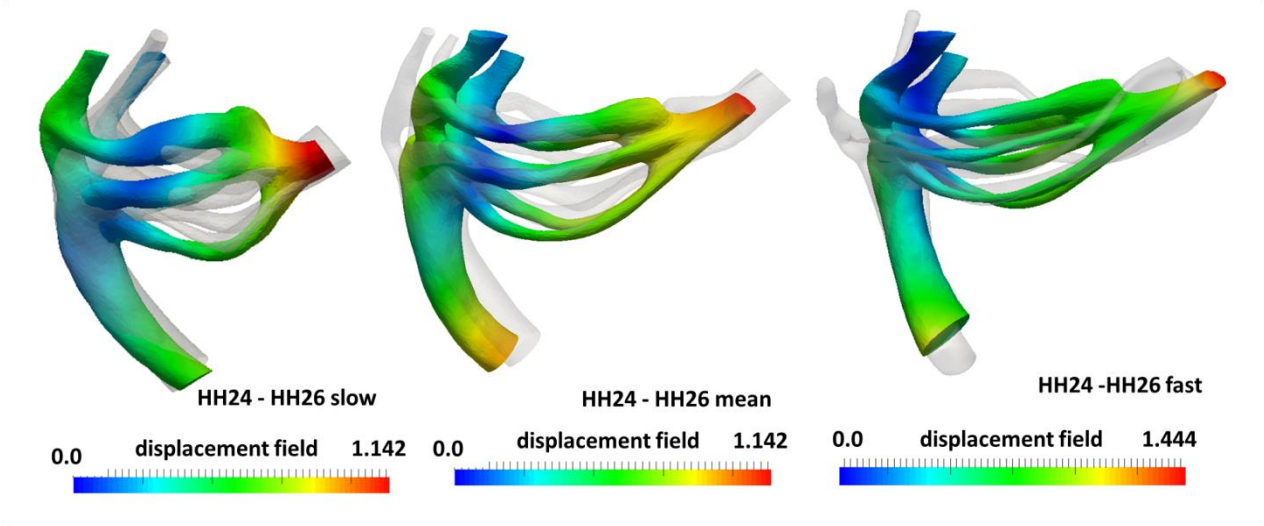

Figure S6: Displacement fields [cm] for growth bounds associated with Figure 6. Transparent overlays represent desired endpoints for statistical shape modeling software.

Movie S1 is attached as a separate file. The video consists of an ultrasound B-mode of flow traveling through the PAAs of a HH26 embryo. The first frame of the video is shown below with arches outlined in dashed lines and labeled. The OFT is also labeled for ease of visibility in the ultrasound video.